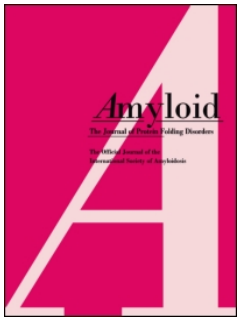

Amyloid
The Journal of Protein Folding Disorders

ISSN: (Print) (Online) Journal homepage: https://www.tandfonline.com/loi/iamy20

Full-length TDP-43 and its C-terminal domain form filaments *in vitro* having non-amyloid properties

Claudia Capitini , Giulia Fani , Mirella Vivoli Vega , Amanda Penco , Claudio Canale , Lisa D. Cabrita , Martino Calamai , John Christodoulou , Annalisa Relini & Fabrizio Chiti

To cite this article: Claudia Capitini , Giulia Fani , Mirella Vivoli Vega , Amanda Penco , Claudio Canale , Lisa D. Cabrita , Martino Calamai , John Christodoulou , Annalisa Relini & Fabrizio Chiti (2020): Full-length TDP-43 and its C-terminal domain form filaments *in vitro* having non-amyloid properties, Amyloid, DOI: 10.1080/13506129.2020.1826425

To link to this article: https://doi.org/10.1080/13506129.2020.1826425

Published online: 07 Oct 2020.

AMYLOID
https://doi.org/10.1080/13506129.2020.1826425

Taylor & Francis
Taylor & Francis Group

ARTICLE

Full-length TDP-43 and its C-terminal domain form filaments *in vitro* having non-amyloid properties

Claudia Capitini[a,b]*, Giulia Fani[a]*, Mirella Vivoli Vega[a], Amanda Penco[c], Claudio Canale[c], Lisa D. Cabrita[d], Martino Calamai[b,e], John Christodoulou[d], Annalisa Relini[c] and Fabrizio Chiti[a]

[a]Section of Biochemistry, Department of Experimental and Clinical Biomedical Sciences, University of Florence, Florence, Italy; [b]European Laboratory for Non-linear Spectroscopy, Sesto Fiorentino, Italy; [c]Department of Physics, University of Genoa, Genoa, Italy; [d]Institute of Structural and Molecular Biology, UCL and Birkbeck College London, London, UK; [e]National Institute of Optics, National Research Council, Sesto Fiorentino, Italy

ABSTRACT

Accumulation of ubiquitin-positive, tau- and α-synuclein-negative intracellular inclusions of TDP-43 in the central nervous system represents the major hallmark correlated to amyotrophic lateral sclerosis (ALS) and frontotemporal lobar degeneration with ubiquitin-positive inclusions (FTLD-U). Such inclusions have variably been described as amorphous aggregates or more structured deposits having amyloid properties. Here we have purified full-length TDP-43 (FL TDP-43) and its C-terminal domain (Ct TDP-43) to investigate the morphological, structural and tinctorial features of aggregates formed *in vitro* by them at pH 7.4 and 37 °C. AFM images indicate that both protein variants show a tendency to form filaments. Moreover, we show that both FL TDP-43 and Ct TDP-43 filaments possess a largely disordered secondary structure, as ascertained by far-UV circular dichroism and Fourier transform infrared spectroscopy, do not bind Congo red and induce a very weak increase of thioflavin T fluorescence, indicating the absence of a clear amyloid-like signature.

Abbreviations: AFM: atomic force microscopy; ALS: amyotrophic lateral sclerosis; CD: circular dichroism; CR: Congo red; Ct TDP-43: C-terminal TDP-43 (residues 274-414); CTD: C-terminal domain; DTT: dithiothreitol; EDTA: ethylenediaminetetraacetic acid; FL TDP-43: full-length TDP-43 (construct PelB-TDP-43$_{1-414}$-His$_6$); FTIR: Fourier transform infra-red spectroscopy; FTLD-U: frontotemporal lobar degeneration with ubiquitin-positive inclusions; HEPES: 4-(2-hydroxyethyl)-1-piperazineethanesulfonic acid; His$_6$: hexahistidine tag; HypF-N: N-terminal domain of the *E. coli* hydrogenase maturation factor HypF; IBs: bacterial inclusion bodies; LLPS: liquid-liquid phase separation; MBP: maltose binding protein; MW: molecular weight; MWCO: molecular weight cut-off; N_2: nitrogen; NTD$_{1-76}$: N-terminal domain; PK: proteinase K; RRM1$_{106-176}$ and RRM2$_{191-259}$: RNA recognition motifs; SDS-PAGE: sodium dodecyl sulphate-polyacrylamide gel electrophoresis; TDP-43: TAR DNA-binding protein 43; TEM: transmission electron microscopy; ThS: thioflavin S; ThT: thioflavin T

ARTICLE HISTORY
Received 21 February 2020
Revised 31 July 2020
Accepted 17 September 2020

KEYWORDS
Motor neuron disease; TDP-43 fibrils; TDP-43 filaments; protein misfolding; protein aggregation

Introduction

Amyotrophic lateral sclerosis (ALS) and frontotemporal lobar degeneration with ubiquitin-positive inclusions (FTLD-U) are progressive and fatal neurodegenerative diseases with patients variably affected by motor, behavior, and cognitive deficits [1,2]. Both sporadic ALS and FTLD-U, as well as most of familial cases of the same diseases, have a characteristic histopathology with polyubiquitinated, hyperphosphorylated and partially proteolyzed cytosolic inclusions containing the TAR DNA-binding protein 43 (TDP-43) [1–4].

TDP-43 is a complex protein of 414 amino acid residues, which is ubiquitously and abundantly expressed in almost all tissues, including neurons of the central nervous system [5]. It consists of an N-terminal domain (NTD$_{1-76}$) with a well-defined fold and shown to trigger the dimerization or oligomerization of the whole protein, two highly conserved folded RNA recognition motifs (RRM1$_{106-176}$ and RRM2$_{191-259}$) and a low complexity, intrinsically disordered C-terminal domain (CTD$_{274-414}$) [6].

Under physiological conditions, TDP-43 normally resides in the nucleus, but shuttles regularly from this cellular compartment to the cytosol [7]. Under pathological conditions, however, the nucleus becomes depleted of TDP-43, which accumulates and forms well defined inclusions in the cytosol [2,8,9]. In such cytoplasmic inclusions, TDP-43 is hyperphosphorylated, ubiquitinated and in part cleaved to form C-terminal fragments [1,2,9], although in the spinal cord motor neurons the inclusions consist exclusively of full-length TDP-43 [4].

The elucidation of the structural, functional, and aggregation properties of TDP-43 has been limited by technical

CONTACT Fabrizio Chiti fabrizio.chiti@unifi.it Section of Biochemistry, Department of Experimental and Clinical Biomedical Sciences, University of Florence, Florence, Italy
*These authors contributed equally to this work.

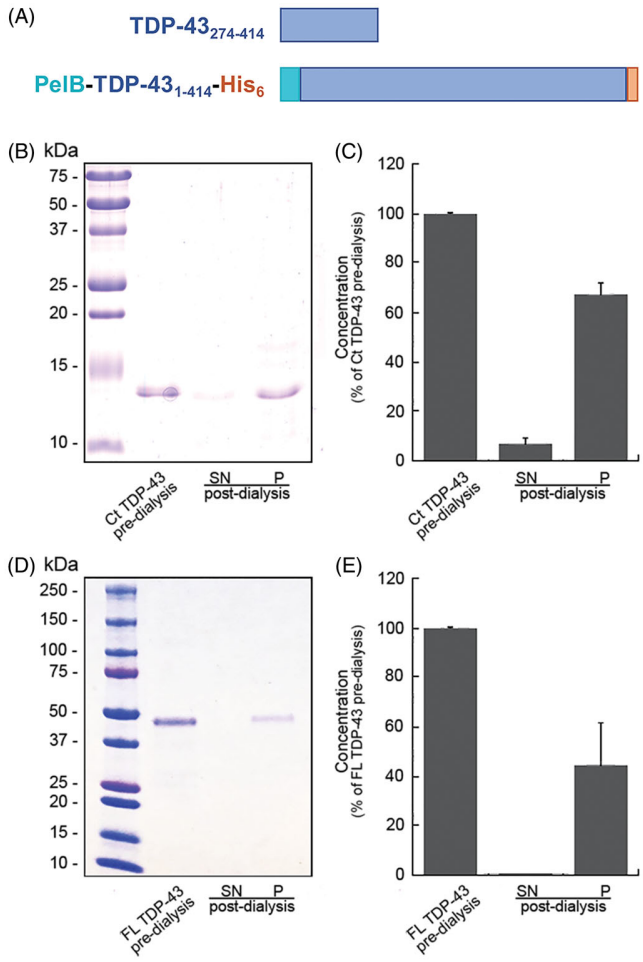

Figure 1. SDS-PAGE analysis of Ct TDP-43 and FL TDP-43 samples pre- and post-dialysis. (A) Schematic representation of the constructs, namely TDP-$43_{274-414}$ and PelB-TDP-43_{1-414}-His_6, referred here as the Ct and FL TDP-43. PelB and His_6 tags had sequences MKYLLPTAAAGLLLLAAQPAMA and ENLYFQSHHHHHH before Met1 and after Met414 of TDP-43, respectively. (B,D) SDS-PAGE analysis of (B) Ct TDP-43 and (D) FL TDP-43 before dialysis (lane 2) and after dialysis for the supernatant (lane 3) and pellet (lane 4) fractions. (C,E) Densitometry analysis expressed in percentage of the bands of (C) Ct TDP-43 and (E) FL TDP-43 in the supernatant (bar 2) and pellet (bar 3) fractions with respect to the pre-dialysis sample (bar 1) that represents the 100% by normalization.

difficulties in purifying the full-length protein to a sufficiently high yield, due to its intrinsic tendency to aggregate and be proteolyzed within the C-terminal domain during the various purification steps [10]. The morphology and structure of TDP-43 in aggregates formed *in vitro* as well as in the mature inclusions of ALS and FTLD-U patients are unclear. In particular, it is not yet clarified whether TDP-43 inclusions have the characteristic order and cross-β structure typical of amyloid fibrils or rather another type of molecular architecture.

To be classified as amyloid, protein aggregates need to satisfy three main criteria: the presence of a fibrillar morphology with the fibrils having a diameter of typically 7–13 nm, the ability to bind amyloid-diagnostic dyes, such as Congo red (CR), thioflavin T (ThT), thioflavin S (ThS) or their derivatives, and the presence of a cross-β secondary structure [11]. Spinal cord sections of ALS patients and brain specimen of FTLD-U cases show the presence of TDP-43 positive, 10–20 nm wide filaments in the absence of binding of the amyloid-diagnostic dyes CR and ThS, thus, suggesting non-amyloid properties [3,12–18]. However, another more recent report indicates the presence of a widespread remarkable ThS staining in TDP-43 inclusions in spinal cords and brains of ALS and FTLD-U cases, respectively, suggesting rather an amyloid-like structure [19]. In another report, it was shown that a few TDP-43 inclusions of ALS patients may consist of 10–20 nm filaments able to bind ThS, but such features were found only in a small fraction of skein-like inclusions of the spinal cord, with amyloid-like characteristics being absent in most spinal cord skeins and absent altogether in other TDP-43 inclusions of the spinal cord and in all inclusions of the brain [20].

Studies of the conversion of full-length (FL) TDP-43 into protein aggregates *in vitro* have appeared very recently, although using large constructs where the TDP-43 protein is fused to large soluble tags [14,21–23]. In the only report where the final aggregates were studied in some detail, a non-amyloid structure with disordered secondary structure and inability to bind ThT was found [14]. A report of FL TDP-43 in the absence of any tags appeared in 2009 and showed that the protein forms filaments unable to bind CR and ThT [24]. By contrast, a number of studies involving the CTD of TDP-43 or even very short fragments of the CTD have shown a well-defined fibrillar morphology with significant ThT fluorescence increase [25–30], leading many investigators in the field to assume that the full-length protein also forms amyloid-like fibrils.

To address this issue, we took advantage of our ability to purify FL TDP-43 to a reasonably high yield [6], in addition to its CTD, and investigated the morphological, structural and tinctorial nature of the aggregates formed *in vitro* by both FL TDP-43 and its CTD.

Methods

Ct and FL TDP-43 purification

TDP-$43_{274-414}$ was expressed as a hexahistidine tagged (His_6) maltose binding protein (MBP) fusion protein and purified from the cytosol of *E. coli*. Following protein expression and cell lysis, the His_6-MBP-TDP-$43_{274-414}$ fusion was purified *via* nickel iminodiacetic acid chromatography using gravity flow. The TDP-$43_{274-414}$ fragment was subsequently cleaved from the His_6-MBP using TEV protease. The resulting aggregates were dissolved in 25 mM Na_2HPO_4, 150 mM NaCl, 5 mM EDTA, 5 mM β-mercaptoethanol, 8 M urea, pH 7.5, and purified further using size exclusion chromatography.

Bacterial inclusion bodies (IBs) containing PelB-TDP-43_{1-414}-His_6 were purified from the insoluble fractions obtained after the cell lysis step, as previously described [6]. The bacterial pellet (~1 g) was subjected to three washes with 50 mM HEPES, pH 8.0, 1% Triton X-100 (wash 1); 50 mM HEPES, pH 8.0, 2 M NaCl (wash 2); 50 mM HEPES, pH 8.0, in the absence of salts (wash 3). After each wash, the mixture was centrifuged at 24,000 *g* for 30 min at 4 °C and the supernatants were discarded. The resulting IBs (~480 mg per L of

bacterial culture) were dissolved with 100 mL of denaturing buffer, containing 50 mM HEPES, 0.3 M NaCl, 10 mM imidazole, 5 mM DTT and 8 M urea, pH 8.0, under constant stirring for *ca.* 15 h at room temperature. The next day, the solubilized IBs were centrifuged again to remove any debris and loaded onto HisPur™ Ni-NTA resin in a gravity column pre-equilibrated with 50 mM Tris-HCl, 0.5 M NaCl, 8 M urea, and 10 mM imidazole, pH 8.0. The column was washed and eluted with the same buffer containing 25 mM and 300 mM imidazole, respectively. The eluted fractions containing PelB-TDP-$43_{1\text{-}414}$-His_6 were pooled, analyzed by sodium dodecyl sulphate-polyacrylamide gel electrophoresis (SDS-PAGE), concentrated using an ultrafilter (Merck, Darmstadt, Germany) and a 3 kDa molecular weight cut-off (MWCO) membrane and frozen at −20 °C.

Protein concentration was determined by optical absorption spectroscopy using a molar absorption coefficient at 280 nm (ε_{280}) of 17,990 $M^{-1}cm^{-1}$ (molecular weight ~13.7 kDa) and 47,900 $M^{-1}cm^{-1}$ (molecular weight ~48.6 kDa) for TDP-$43_{274\text{-}414}$ and PelB-TDP-$43_{1\text{-}414}$-His_6 (Figure 1(A)), respectively. We will refer to these two protein constructs as Ct TDP-43 and FL TDP-43, respectively.

Ct and FL TDP-43 aggregation

Aliquots of 60 µL and 410 µL of denatured Ct and FL TDP-43, respectively, both at a protein concentration of 1.5 mg/mL (corresponding to a molar concentration of 109.5 µM and 30.9 µM, respectively), were prepared, and 10 µL of each sample at the same concentration (1.5 mg/mL) were analyzed with SDS-PAGE using 12% (w/v) polyacrylamide gels. The remaining samples were dialyzed overnight, using a membrane with a MWCO of 12.4 kDa, at 37 °C against 4.0 L of 50 mM NaH_2PO_4, 1 mM DTT, pH 7.4, to remove urea and other components and promote their aggregation. After dialysis, 10 µL of samples were centrifuged and the presence of protein in the pellet and supernatant fractions was checked by SDS-PAGE, using 12% (w/v) polyacrylamide gels, and the bands quantified with the ImageJ software (NIH Image J System, Bethesda, MD). Other 10 µL of samples were centrifuged and the pellet fractions were resuspended in 10 µL of 50 mM NaH_2PO_4, 1 mM DTT, pH 7.4, immediately before any measurement, so that the original concentration was maintained. In the following experiments, the reported protein concentrations are always referred to the monomeric pre-dialysis protein concentration.

HypF-N purification and aggregation

The N-terminal domain of the *E. coli* protein HypF (HypF-N, 11 kDa) was purified as previously reported [31]. It was incubated for one week at a concentration of 0.8 mg/mL in 50 mM acetate buffer, 30% (v/v) TFE, pH 5.5, room temperature. It was then diluted to 0.25 mg/mL into the same buffer immediately before the ThT and CR assays described below.

AFM

Ct and FL TDP-43 were prepared and dialyzed as described above. After dialysis, a 20 µL aliquot of the whole sample (1.5 mg/mL) was deposited on freshly cleaved mica, incubated for 10 min, gently rinsed with MilliQ water and dried under mild vacuum. Diluted samples were also prepared by diluting 5 µL aliquots of the dialyzed sample (1.5 mg/mL) 100 and 1000 times. A 10 µL aliquot of each diluted sample was deposited and treated as described above. Tapping mode AFM images were acquired in air using a Dimension 3100 SPM (Bruker, Karlsruhe, Germany) equipped with "G" scanning head (maximum scan size 100 µm) and driven by a Nanoscope IIIa controller (Bruker, Karlsruhe, Germany), and a Multimode SPM (Bruker) equipped with "E" scanning head (maximum scan size 15 µm) and driven by a Nanoscope V controller (Bruker, Karlsruhe, Germany). Single beam uncoated silicon cantilevers (type OMCL-AC160TS, Olympus, Tokyo, Japan) were used. The drive frequency was 270–300 kHz and the scan rate was 0.3–0.7 Hz.

Aggregate heights and widths were measured from the cross section profiles of topographic AFM images. Sections were traced perpendicularly to the filament axis. The measured apparent widths were corrected for the tip-induced broadening in the image plane according to $w_{measurement} - w_{real} = 2\sqrt{2Rh} - h$, where h is the measured object height and R is the AFM tip radius [32].

ThT fluorescence

Ct and FL TDP-43 aggregates, prepared as described above and then diluted to a concentration of 0.4 mg/mL (29.2 µM and 8.2 µM for Ct and FL TDP-43, respectively), were incubated at 25 °C for 5 min and an aliquot of 60 µL of each sample was mixed with 440 µL of 25 mM NaH_2PO_4 buffer at pH 6.0 containing 25 µM ThT. We decided to use the same mass concentration for FL and Ct TDP-43 aggregates, rather than the same molar concentration, as we considered that having both samples with a similar "protein mass" reduced the possibility of misinterpreting the data obtained. The resulting fluorescence was measured at 25 °C using a Perkin-Elmer LS 55 spectrofluorimeter (Waltham, MA), using excitation and emission wavelengths of 440 and 450–600 nm, respectively. A 2 × 10 mm quartz cuvette was used. For FL TDP-43 aggregates, the ThT fluorescence measurements were also collected after 1, 2, 5, 6, 7, and 8 days from the beginning of dialysis when the aggregates start to form, keeping the original sample at 0.4 mg/mL protein at 37 °C between the different measurements. The experiment was repeated using HypF-N aggregates, prepared as described above and diluted to a concentration of 0.25 mg/mL at 25 °C for 5 min before the assay.

CR absorbance

Ct and FL TDP-43 aggregates, prepared as described above and diluted to a concentration of 0.4 mg/mL (29.2 µM and

8.2 μM for Ct and FL TDP-43, respectively), were incubated at 25 °C for 5 min and an aliquot of 60 μL of each sample was mixed with 440 μL of 5 mM NaH_2PO_4, 150 mM NaCl buffer at pH 7.4 containing 20 μM CR. Absorbance spectra were recorded from 400 nm to 700 nm using a 5 mm quartz cell and a Jasco V-630 spectrophotometer (Tokyo, Japan). Spectra of similar samples devoid of CR and of similar samples devoid of aggregates were also recorded. The spectrum of CR bound to β-sheet structure was obtained by subtracting the spectra of CR alone and TDP-43 aggregates alone from that of CR and TDP-43 aggregates. For FL TDP-43 aggregates, CR spectra were also acquired after 1, 2, 5, 6, 7, and 8 days from beginning of dialysis, keeping the original sample at 0.4 mg/mL protein at 37 °C between the measurements. The experiment was repeated using HypF-N aggregates, prepared as described above and diluted to 0.25 mg/mL at 25 °C for 5 min before the assay.

Far-UV CD

Ct and FL TDP-43 aggregates were prepared as described above and diluted to 0.2 mg/mL (14.6 μM) and 0.05 mg/mL (1.0 μM) protein concentrations, respectively. The far-UV circular dichroism (far-UV CD) spectra were collected over the 190–260 nm wavelength range at 25 °C using a Jasco J-810 Spectropolarimeter (Tokyo, Japan). A 1 mm path-length cell was used. All spectra were blank subtracted.

FTIR

Ct and FL TDP-43 aggregates were prepared as described above at 1.5 mg/mL protein concentration (109.5 μM and 30.9 μM for Ct and FL TDP-43, respectively). They were then centrifuged twice at 12,000 *g*, 4 °C, for 10 min and resuspended in both cases in D_2O to a final protein concentration of 10 mg/mL. Each sample was deposited on a KBr window in a semipermanent liquid cell using a 25 μm spacer, and the Fourier transform infra-red spectroscopy (FTIR) spectrum was recorded at room temperature using a Jasco FTIR 4200 spectrophotometer (Tokyo, Japan). The system was constantly purged with N_2. The resulting spectra were background subtracted and baseline corrected.

PK digestion of FL TDP-43 filaments

FL TDP-43 aggregates were prepared as described above at 1.5 mg/mL (30.9 μM) protein concentration. They were then digested with 5 μg/mL proteinase K (PK) at 37 °C for 20 min and 10 μL were analyzed with SDS-PAGE using 12% (w/v) polyacrylamide gels. The remaining sample was centrifuged, and the pellet was resuspended in the same volume of 50 mM NaH_2PO_4, 1 mM DTT, pH 7.4 to maintain the original concentration and analyzed with CR assay and CD spectroscopy, as described above.

Results

Formation of Ct TDP-43 and FL TDP-43 aggregates

Ct TDP-43 and FL TDP-43 were purified under denaturing conditions, as described in the *Methods* section "*Ct and FL TDP-43 purification*." The resulting constructs are described in Figure 1(A). The denatured proteins (1.5 mg/mL) were first allowed to spontaneously aggregate through a dialysis step against a buffer devoid of urea, i.e. 50 mM NaH_2PO_4, 1 mM DTT, pH 7.4, at 37 °C. Samples were then centrifuged to obtain the pellet and supernatant fractions. Figure 1 reports the SDS-PAGE analysis carried out for both TDP-43 variants before and after dialysis. In the pre-dialysis lane, the Ct TDP-43 band corresponds to a molecular weight of ~13.5 kDa, in agreement with a value of 13.7 kDa expected for the Ct TDP-43 encompassing residues 274–414 (Figure 1(B)); the FL TDP-43 band corresponds to a molecular weight of ~48 kDa, in agreement with a value of 48.6 kDa expected for TDP-43 including PelB and His_6 tags (Figure 1(D)). Ct TDP-43 was found in the pellet fraction after dialysis with a percentage of 67 ± 5% of the initial protein (Figure 1(B,C)). A mild band was also observed in the supernatant fraction (6 ± 4%), suggesting that not all protein undergoes aggregation. Moreover, some protein (*ca.* 27%) was lost because of its early aggregation on the membrane during dialysis. Rather, FL TDP-43 was found entirely in the pellet fraction after dialysis, although the band intensity was 45 ± 16% of that found before dialysis (Figure 1(D,E)); similar to the Ct TDP-43 case, the remaining *ca.* 55% was found to prematurely accumulate on the dialysis membrane.

Ct TDP-43 and FL TDP-43 form filaments and assemblies resembling liquid droplets

Ct TDP-43 and FL TDP-43 were purified under denaturing conditions and dialyzed overnight to remove urea, as described above. The resulting samples were deposited on mica, dried and analyzed with AFM. The Ct TDP-43 sample was found to contain many large spherical enclosures with a diameter of the μm order containing inside smaller particles, possibly representing patches of dried protein (Figure 2(A)). Patterns of this type have been attributed to liquid droplets originating from liquid–liquid phases separation (LLPS) [25] and occasionally appeared to coalesce (Figure 2(A)). The sample also contained many filaments mostly intertwined into larger assemblies (Figure 2(B,C)). The FL TDP-43 sample also appeared to consist of mixtures of filaments and possible dried droplets (Figure 2(D–F)), although the droplets were more compact and smaller in diameter (Figure 2(D,F)), again similar to some of the compact round particles previously reported [25].

Figure 3 reports further details of Ct TDP-43 and FL TDP-43 aggregates. In the Ct TDP-43 sample, relatively thin filaments with no apparent twist (Figure 3(A), solid white arrows) coexisted with larger, twisted fibrils (Figure 3(A), black arrows), also forming large bundles. Only a few number of thin filaments were found in the sample (Figure 3(A), dashed white arrow). The height distribution of the thin

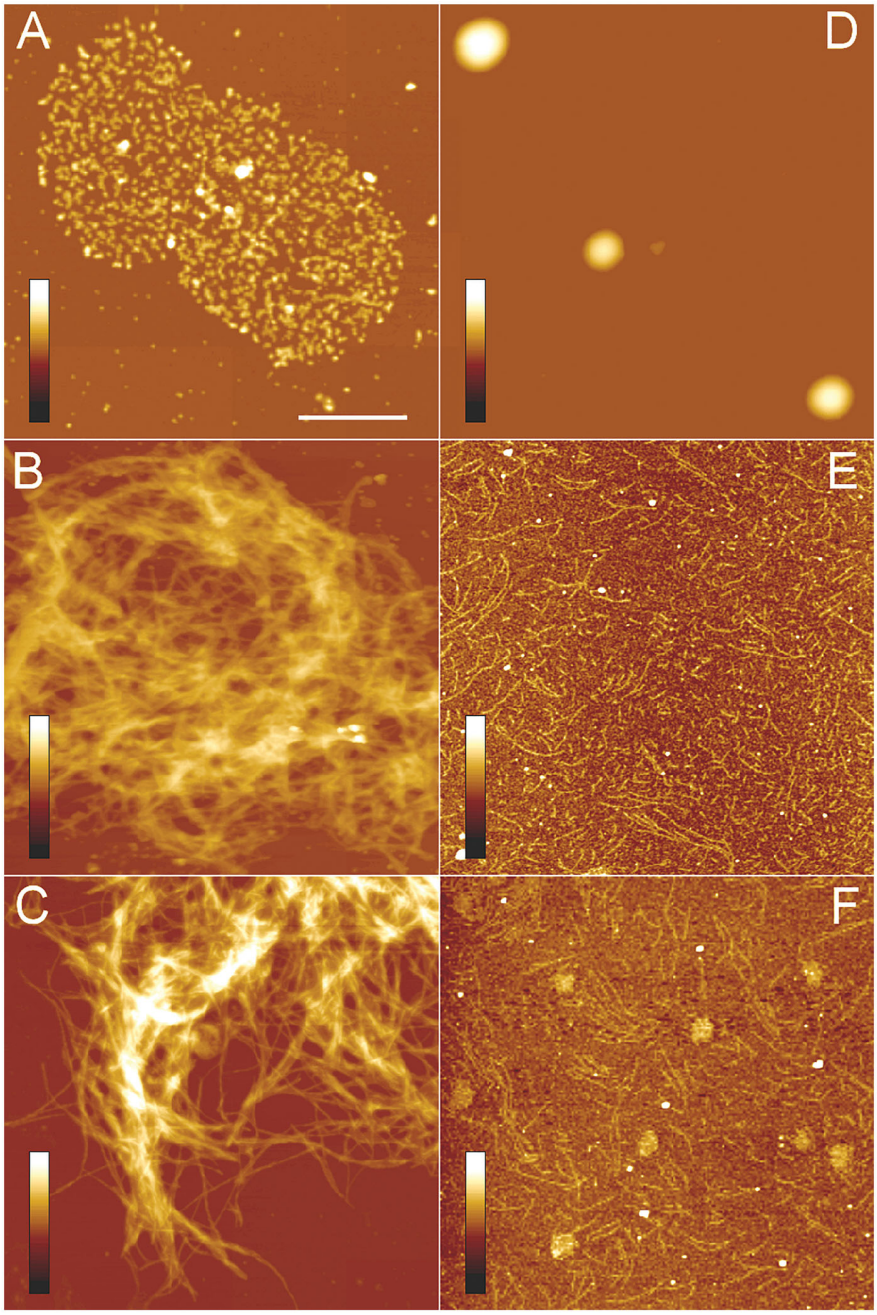

Figure 2. AFM analysis of Ct TDP-43 and FL TDP-43 aggregates. Tapping mode AFM images (height data) of (A–C) Ct TDP-43 and (D–F) FL TDP-43 aggregates obtained after dialysis. Scan size 4.0 μm. The scale bar corresponds to 1 μm. Z range: (A) 300 nm, (B) 35 nm, (C) 100 nm, (D) 150 nm, (E) 4.0 nm, and (F) 5.0 nm.

untwisted filaments (Figure 3(A), inset) has a mean of 4.2 ± 0.1 nm (mean ± standard error). The smallest untwisted filaments had heights between 0.8 and 1.8 nm (corresponding to the left tail of the distribution in Figure 3(A)), whereas the larger twisted fibrils were 7–10 nm in height. Typical height profile of the three types of filaments are shown in Figure 3(C,D). In the FL TDP-43 sample, filaments with a height of 1.2 ± 0.1 nm (mean ± standard error), compatible with the size of the smallest structures observed for Ct TDP-43, were observed (Figure 3(B)). The three major peaks in the height profile correspond to filaments, while other peaks are associated with protein oligomers, which cover the image background (Figure 3(E)). FL TDP-43 filaments did not exhibit the tendency found for Ct TDP-43 filaments to associate into twisted structures. The filament width is 35 ± 5 nm. This value is larger than those reported from transmission electron microscopy (TEM) measurements [3,12,13,16,17,20,24], due to overestimation of the AFM-derived fibril width as a fibril diameter due to tip-sample convolution effects, as discussed below.

Ct TDP-43 and FL TDP-43 aggregates do not bind CR and ThT

We then analyzed the capacity of the samples to bind the amyloid-specific dye ThT and increase its fluorescence. Ct

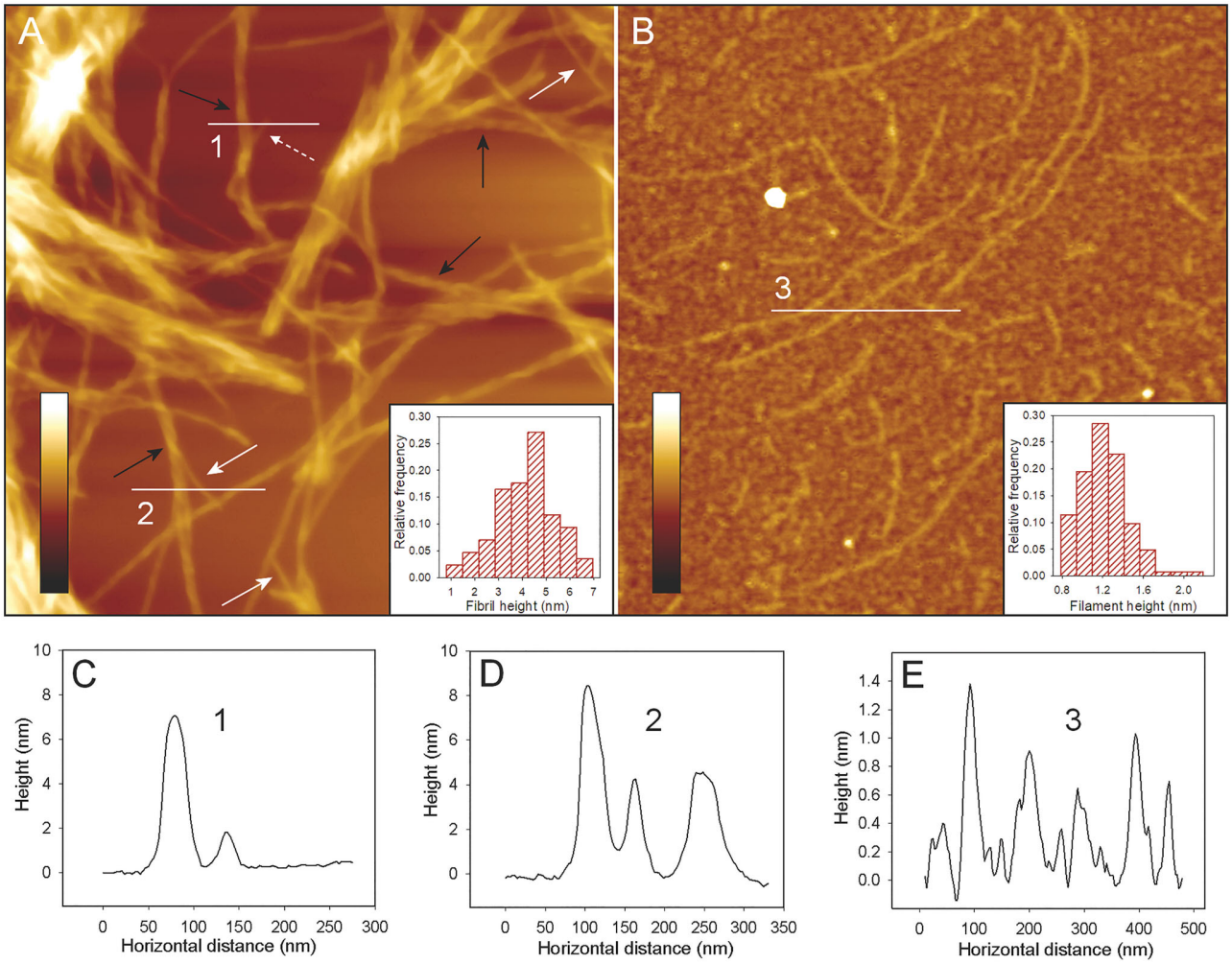

Figure 3. AFM analysis and size determination of Ct TDP-43 and FL TDP-43 aggregates. Tapping mode AFM images (height data) of (A) Ct TDP-43 filaments and (B) FL TDP-43 filaments. In (A) examples of twisted fibrils, thin filaments with no evident twist and very thin filaments are indicated by black arrows, solid white arrows and dashed white arrows, respectively. Scan size 1.5 µm. Z range: (A) 60 nm and (B) 8.0 nm. Insets, height distributions of (A) Ct TDP-43 thin filaments and (B) FL TDP-43 filaments. (C–E) Representative height profiles along the corresponding white lines in (A) and (B). In (E), the three highest peaks correspond to filaments, while other peaks correspond to protein oligomers, which cover the image background.

TDP-43 and FL TDP-43 were purified under denaturing conditions and dialyzed overnight to remove urea, as described above. The resulting samples were centrifuged and their pellets resuspended and analyzed. The ThT fluorescence increases to a small extent in the presence of Ct TDP-43 and FL TDP-43 aggregates, by *ca.* 2.6 and 2.2 times, respectively (Figure 4(A,B)). We repeated the assay using amyloid-like fibrils formed from the protein HypF-N as a positive control [33,34] and found a *ca.* 7.5-fold ThT fluorescence increase (Figure 4(C)). Since amyloid-like fibrils generally induce an increase of the dye fluorescence emission by over 5-fold [35], we can infer that the Ct and FL TDP-43 filaments formed after dialysis do not show a typical amyloid-like behavior. ThT fluorescence in the presence of FL TDP-43 aggregates did not increase linearly or exponentially over the subsequent 8 days (Figure 4(D)), ruling out the formation of amyloid-like species upon prolonged incubation.

We then used the amyloid diagnostic CR dye to assess the ability of the samples to bind it and cause a red-shift of its maximum optical absorption [36]. The CR absorbance spectra obtained in the presence and absence of Ct TDP-43 or FL TDP-43 aggregates are nearly superimposable, with a maximum absorption at ~490 nm (Figure 4(E,F)). The difference spectrum, obtained by subtracting the CR spectrum and the TDP-43 aggregates spectrum from the CR spectrum in the presence of TDP-43 aggregates, was flat in both cases, without a peak at 540 nm expected for CR bound to amyloid-like fibrils (Figure 4(E,F)), indicating that Ct and FL TDP-43 aggregates do not show any amyloid-like features in standard dye-based assays. By contrast, amyloid-like fibrils formed from HypF-N, used here as a positive control [33,34], showed the typical peak at 540 nm in the difference spectrum (Figure 4(G)). The difference spectra recorded for the FL TDP-43 aggregates over 8 days were flat, suggesting that amyloid-like fibrils do not form over time (Figure 4(H)).

To rule out the possibility that TDP-43 filaments have an amyloid core formed by a small portion of its sequence that is buried inside and masked by exposed flexible regions, we treated FL TDP-43 aggregates with PK to disrupt the disordered portions of the aggregate and to expose, if existing,

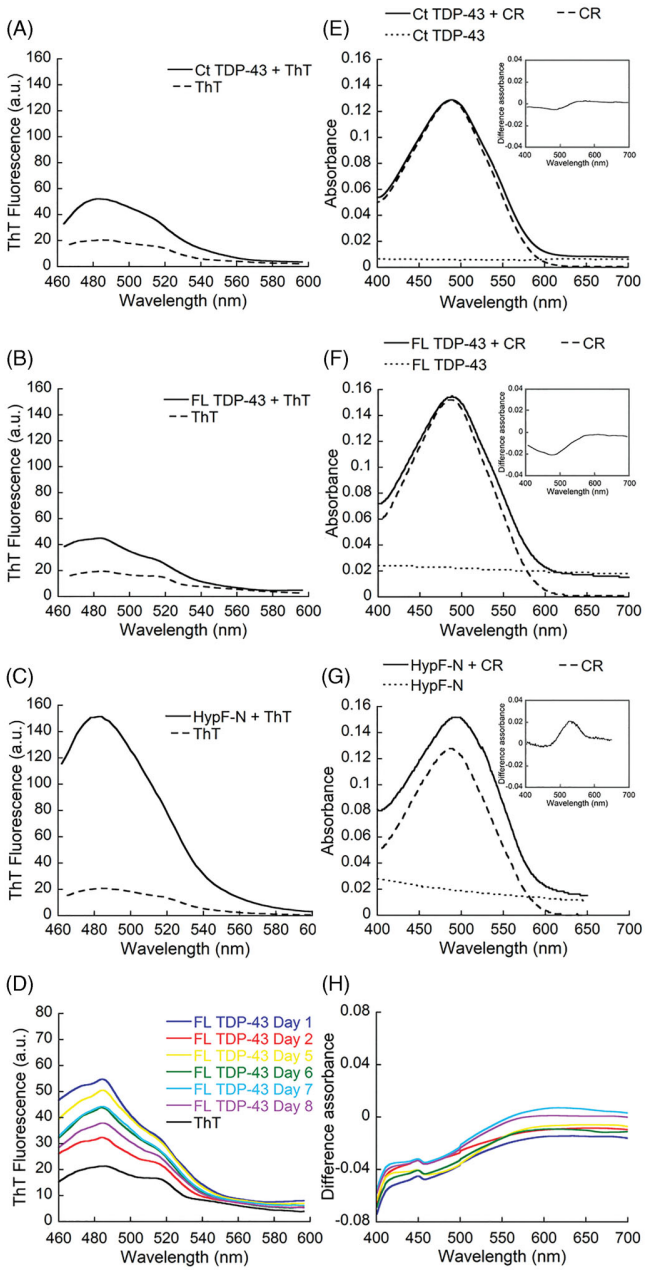

Figure 4. ThT and CR binding of Ct TDP-43 and FL TDP-43 aggregates. (A,B,C) ThT fluorescence spectra in the presence (solid line) or absence (dashed line) of (A) Ct TDP-43 aggregates, (B) FL TDP-43 aggregates and (C) HypF-N amyloid-like fibrils as a positive control. HypF-N has a molecular weight of 11 kDa. (D) ThT fluorescence spectra in the presence of FL TDP-43 aggregates after the indicated time of incubation from the beginning of dialysis. (E,F,G) Absorbance spectra of protein aggregates and CR (solid line), CR alone (dashed line) and protein aggregates alone (dotted line) for (E) Ct TDP-43 aggregates, (F) FL TDP-43 aggregates and (G) HypF-N amyloid-like fibrils as a positive control. In all cases, the difference spectra (insets) were obtained by subtracting the spectra of CR alone and aggregates alone from that of CR and aggregates. (H) CR difference spectra of FL TDP-43 aggregates after the indicated time of incubation from the beginning of dialysis.

the resistant amyloid core. SDS-PAGE analysis showed the disappearance of the 48 kDa FL TDP-43 band and the emergence of a new main band at *ca.* 15 kDa and another weak band at *ca.* 8 kDa (data not shown). The difference spectrum was again flat, excluding any evidence of an amyloid core inside the aggregates (data not shown).

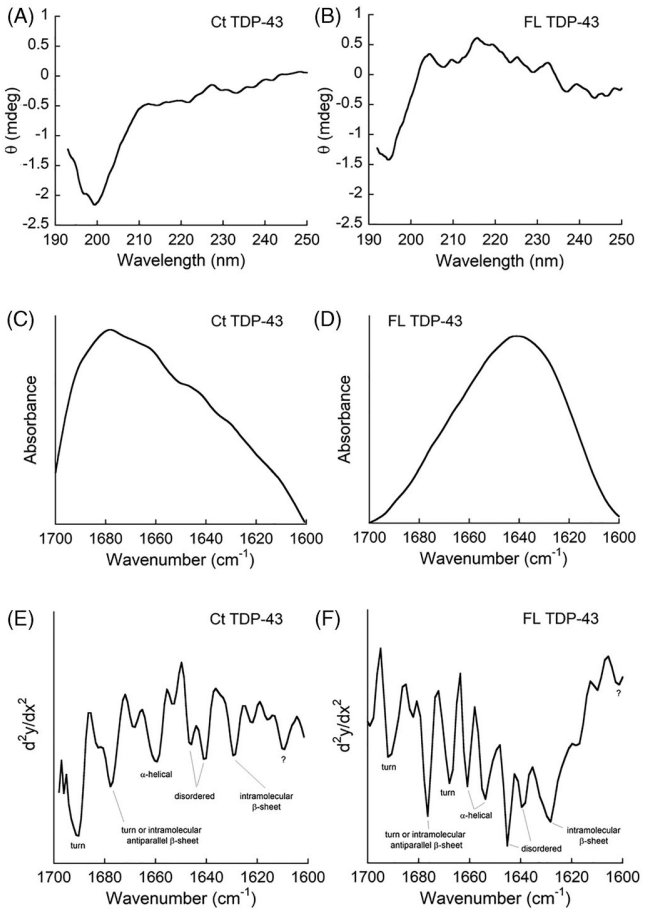

Figure 5. Secondary structure analysis of Ct TDP-43 and FL TDP-43 aggregates. (A,B) Far-UV CD spectra of Ct TDP-43 (A) and FL TDP-43 (B) aggregates. Spectra were blank subtracted. (C,D) Amide I regions of FTIR spectra of Ct TDP-43 (C) and FL TDP-43 (D) aggregates. The spectra were background subtracted, baseline corrected and smoothed. (E,F) Second derivative of the FTIR spectra of Ct TDP-43 (E) and FL TDP-43 (F) aggregates. Negative peaks were assigned as indicated.

Ct TDP-43 and FL TDP-43 aggregates consist of a random coil structure

A distinctive characteristic of amyloid fibrils is the β-sheet content that can be typically detected by means of a number of techniques, such as far-UV CD, FTIR, and X-ray fiber diffraction [37,38]. The far-UV CD spectrum of Ct TDP-43 aggregates, prepared as described above, shows a negative peak at *ca.* 198 nm (Figure 5(A)), which is indicative of aggregates having a random coil content. Although more noisy, a similar far-UV CD spectrum was obtained for FL TDP-43 aggregates, with a negative peak at *ca.* 194 nm (Figure 5(B)). FL TDP-43 aggregates treated with PK showed a flat CD spectrum without any peak corresponding to a β-sheet secondary structures (data not shown).

The amide I region of the FTIR spectrum of Ct TDP-43 aggregates obtained in D_2O shows a prominent peak at $\sim$1680 cm^{-1} (Figure 5(C)). The second derivative spectrum reveals major peaks at $\sim$1691 cm^{-1} and $\sim$1677 cm^{-1} associated with β-turn structure or intramolecular antiparallel β-sheet structure, a minor peak at $\sim$1660 cm^{-1}, assignable to α-helical structure, at 1646 and 1641 cm^{-1}, arising from unordered structure, and at 1630 cm^{-1}, attributable to

intramolecular β-sheet structure (Figure 5(E)). This FTIR spectrum is non-canonical as it is dominated by a large band around 1680 cm^{-1}, but is very similar to that previously obtained for bacterial IBs enriched with Ct TDP-43 [10]. The FTIR spectrum of FL TDP-43 aggregates was found to display a dominant peak at ~1640 cm^{-1}, corresponding to largely unordered structure (Figure 5(D)). The second derivative spectrum also reveals major peaks at 1645 and 1640 cm^{-1}, arising from unordered structure, and other peaks at ~1655 and 1661 cm^{-1}, assignable to α-helical structure, ~1629 cm^{-1}, attributable to intramolecular β-sheet structure, ~1692 cm^{-1}, ~1677 cm^{-1} ~1668 cm^{-1}, associated with β-turn structure or intramolecular antiparallel β-sheet structure (Figure 5(F)).

Overall, the far-UV CD and FTIR results provide evidence for the lack of significant intermolecular β-sheet structure and for the presence of largely disordered secondary and turn structure in both variants of TDP-43 aggregates.

Discussion

In this work, we have dialyzed the Ct and FL variants of TDP-43, maintained initially soluble in 8 M urea, against a buffer solution at neutral pH and 37 °C in the absence of urea, which is a condition known to promote both LLPS and aggregation of both Ct TDP-43 and FL TDP-43 fused to large tags [10,14,21,25,26,39–41]. After the dialysis process, followed by a centrifugation step, the two protein samples were predominantly found in the pellet, indicating that in both cases the soluble protein had converted into self-assembled species that had a density higher than that of the bulk solution. The resuspended pellets were then studied with methods to monitor their structure and tinctorial properties, whereas the whole post-dialysis sample was used to analyze its morphology. Although FL TDP-43 contained the PelB and His_6 tags, these were very short and were expected to change only marginally the aggregation properties of the full-length protein [6].

AFM images are indicative of Ct and FL TDP-43 liquid droplets

One important aspect of TDP-43 is its tendency to undergo LLPS, which is a process driven by the Ct domain [14,21–23,25,39–42]. LLPS was observed *in vitro* for the isolated Ct domain under various conditions, including those of pH, protein concentration and salt concentration studied here [25,39–42]. LLPS was also observed more recently for FL TDP-43 fused to solubilizing large tags, such as the yellow fluorescent protein [14], the maltose binding protein [21,22] and the small ubiquitin-like modifier [22,23], again under similar conditions to those studied here. LLPS of TDP-43 is also thought to have physiological relevance, because TDP-43 containing stress granules (SGs), that form *in vivo* as sites of stalled mRNA translation under conditions of stress, have characteristics of a liquid phase [43], although cytoplasmic liquid droplets of TDP-43 and stress granules can form independently of each other [39].

The AFM images shown in Figure 2(A) are indicative of LLPS for the Ct domain, as they show large droplets deposited and dried on a mica surface appearing as large spherical enclosures of the μm order containing shrinked protein particles within them, as has been found previously in closely similar AFM images [25]. The AFM images are also indicative of LLPS for FL TDP-43 (Figure 2(D,F)). In this case, the images indicate more compact spherical structures, again similar to the round particles previously reported [25].

Filaments of Ct and FL TDP-43 show non-amyloid properties

Both samples of Ct and FL TDP-43 indicated significant filament formation (Figures 2 and 3). The width measured with AFM for the FL TDP-43 filaments, as well as the thinner untwined filamentous structures of Ct TDP-43, was found to be 35 ± 5 nm. This value is slightly larger than the diameter measured for TDP-43 filaments found in neuronal inclusions, which is typically 10–20 nm, as observed with TEM [3,12,13,16,17,20]. It is also larger than that measured with TEM for TDP-43 filaments *in vitro* [24,44]. This difference is likely to arise from tip-sample convolution effects, which tends to overestimate the width when measured with AFM. Ct TDP-43 filaments (Figures 2(B,C) and 3(A)), but not FL TDP-43 filaments (Figures 2(E,F) and 3(B)), were found to associate into twisted structures. The longer sequence and larger complexity of FL TDP-43 probably make the structure formed by the polypeptide chain more disordered but also able to expose a sufficient amount of hydrophilic surfaces.

Far-UV CD and FTIR spectroscopies indicated that these filaments contained predominantly disordered secondary structure (Figure 5). The two samples analyzed could not cause the characteristic red shift from 490 nm to 540 nm of the optical absorption peak of CR (Figure 4(E,F)) as observed for fibrils with an amyloid-like nature [36]. Moreover, they could induce only a weak increase of ThT fluorescence at 485 nm (Figure 4(A,B)), which is significantly lower than that observed in the case of fibrils with amyloid-like structure, which is at least 5-fold [35]. These techniques can report on both droplets, that are known to contain protein molecules in a disordered structure [43], and filaments, as they both coexist in our samples. However, the time-courses of ThT fluorescence and CR absorption indicate that the spectral properties of the samples do not change with time as the filaments accumulate (Figure 4(D,H)); in addition, the samples are dominated by filaments even after dialysis ruling out the possibility that the acquired spectroscopic signals arise predominantly from droplets shadowing filaments.

Hence, the absence of a persistent β-sheet structure in the filaments suggests the presence of a propagating interaction between aggregates and individual protein molecules in the absence of a cross-β spine or the presence of a cross-β core involving a very limited portion of the protein

sequence in the presence of a largely disordered surrounding structure.

TDP-43 filaments: amyloid or non-amyloid? A survey of the literature

The finding reported here of a non-amyloid nature of the TDP-43 assemblies is not entirely novel and would have not been surprising to the early structural investigators of TDP-43 aggregates: two reports published in 2009 and 2011 showed that FL TDP-43 can form *in vitro* filaments unable to bind CR and ThT [24], or with very weak ThT binding [44]. Histopathologists also imaged TDP-43 containing filaments, 10–20 nm wide, with TEM within neurons or motor neurons of ALS and FTLD patients [3,12,16,17,20], in the absence of ThT, ThS or CR binding, indicating the presence of a non-amyloid behavior [13,18]. A later report described ThS-positive TDP-43 inclusions in patients, but the ThS positivity was found only in a small fraction of skein-like inclusions of the spinal cord and ThS positivity was entirely absent in other types of spinal cord TDP-43 inclusions and was also not found in the brain independently of the inclusion morphology [20].

However, more recent reports have called the non-amyloid nature of the TDP-43 into question. A diffuse ThS positivity was found in all the analyzed TDP-43 inclusions of ALS spinal cords and FTLD-U brains [19]. Moreover, conditions have been found for the conversion *in vitro* of the low complexity domain of TDP-43 into amyloid-like fibrils [25,26] as well as of short peptides from its sequence [27–30,45] or from that of the RRM2 domain [29,46].

Such observations have caused a paradigm shift and have led to the assumption that even FL TDP-43 may have an amyloid structure in the inclusions. The data presented here show that is not the case and are also supported by other recent findings. For example, Sun and co-workers converted a protein construct consisting of FL TDP-43 fused to the yellow fluorescent protein into reversible aggregated species that had an irregular flocculant morphology unable to bind ThT [14]. The same authors reanalyzed post-mortem FTLD brain specimens and found inclusions positive for TDP-43 but negative for ThS [14]. In an independent earlier study, IBs extracted from *E. coli* following the over-expression of Ct and FL TDP-43 showed a random-coil and β-turn secondary structure, as monitored with CD and FTIR, an inability to bind ThT or CR and a high susceptibility to PK digestion [10].

Can we reconcile these apparently contradictory reports? Small peptides and short sequences are well known to have a high propensity to form amyloid-like fibrils [47,48] and a threshold of protein length has been found between long protein sequences unable to form well-defined amyloid and short ones that, by contrast, can produce such structures [11,49,50]. It is likely that short peptides or domains dissected form the entire sequence of TDP-43 have an ability to form ordered cross-β aggregates. The finding by Bigio and co-workers of a marked ThS positivity in ALS and FTLD-U specimens originated from the chemically harsh treatment of the tissue sections, based on the sequential use of potent oxidants, reductants, acids and bases, such as permanganate, metabisulfite, oxalic acid, sodium hydroxide, and hydrogen peroxide [19], all known to induce conformational changes within proteins, chemically modify them and even hydrolyze their peptide bonds. It cannot be ruled out that the biological inclusions undergo a substantial structural reorganization under such circumstances and even fragmentation, with a higher propensity to form amyloid. The fact remains that in all studies performed *in vitro* on FL TDP-43 [10,14,24,44] and *in vivo* on biological specimens enriched with TDP-43 inclusions [13,14,18,20], a clear amyloid-signature remains undetected.

Disclosure statement

The authors report no conflict of interest.

Funding

This work was supported by a full grant from the Fondazione Italiana di Ricerca per la Sclerosi Laterale Amiotrofica (AriSLA, project TDP-43-STRUCT), by a grant from Università di Firenze – Fondazione Cassa di Risparmio di Firenze (Project TDP43SLA), by the Motor Neuron Disease Association (Grants 6273 & 882-792), Wellcome Trust (206409/Z/17/Z), by the European Union's Horizon 2020 research and innovation programme (654148, Laserlab-Europe), and by University of Genoa (FRA 2018).

References

[1] Neumann M, Kwong LK, Lee EB, et al. Phosphorylation of S409/410 of TDP-43 is a consistent feature in all sporadic and familial forms of TDP-43 proteinopathies. Acta Neuropathol. 2009;117(2):137–149.

[2] Mackenzie IR, Bigio EH, Ince PG, et al. Pathological TDP-43 distinguishes sporadic amyotrophic lateral sclerosis from amyotrophic lateral sclerosis with SOD1 mutations. Ann Neurol. 2007;61(5):427–434.

[3] Hasegawa M, Arai T, Nonaka T, et al. Phosphorylated TDP-43 in frontotemporal lobar degeneration and amyotrophic lateral sclerosis. Ann Neurol. 2008;64(1):60–70.

[4] Igaz LM, Kwong LK, Xu Y, et al. Enrichment of C-terminal fragments in TAR DNA-binding protein-43 cytoplasmic inclusions in brain but not in spinal cord of frontotemporal lobar degeneration and amyotrophic lateral sclerosis. Am J Pathol. 2008;173(1):182–194.

[5] Ou SH, Wu F, Harrich D, et al. Cloning and characterization of a novel cellular protein, TDP-43, that binds to human immunodeficiency virus type 1 TAR DNA sequence motifs. J Virol. 1995;69(6):3584–3596.

[6] Vivoli Vega M, Nigro A, Luti S, et al. Isolation and characterization of soluble human full-length TDP-43 associated with neurodegeneration. Faseb J. 2019;33(10):10780–10793.

[7] Ayala YM, Misteli T, Baralle FE. TDP-43 regulates retinoblastoma protein phosphorylation through the repression of cyclin-dependent kinase 6 expression. Proc Natl Acad Sci USA. 2008; 105(10):3785–3789.

[8] Lee EB, Lee VM, Trojanowski JQ. Gains or losses: molecular mechanisms of TDP43-mediated neurodegeneration. Nat Rev Neurosci. 2011;13(1):38–50.

[9] Neumann M, Sampathu DM, Kwong LK, et al. Ubiquitinated TDP-43 in frontotemporal lobar degeneration and amyotrophic lateral sclerosis. Science. 2006;314(5796):130–133.

[10] Capitini C, Conti S, Perni M, et al. TDP-43 inclusion bodies formed in bacteria are structurally amorphous, non-amyloid and inherently toxic to neuroblastoma cells. PLoS One. 2014; 9(1):e86720
[11] Chiti F, Dobson CM. Protein misfolding, amyloid formation, and human disease: a summary of progress over the last decade. Annu Rev Biochem. 2017;86:27–68.
[12] Lin WL, Dickson DW. Ultrastructural localization of TDP-43 in filamentous neuronal inclusions in various neurodegenerative diseases. Acta Neuropathol. 2008;116(2):205–213.
[13] Kerman A, Liu HN, Croul S, et al. Amyotrophic lateral sclerosis is a non-amyloid disease in which extensive misfolding of SOD1 is unique to the familial form. Acta Neuropathol. 2010; 119(3):335–344.
[14] Sun Y, Medina Cruz A, Hadley KC, et al. Physiologically important electrolytes as regulators of TDP-43 aggregation and droplet-phase behavior. Biochemistry. 2019;58(6):590–607.
[15] Kwong LK, Uryu K, Trojanowski JQ, et al. TDP-43 proteinopathies: neurodegenerative protein misfolding diseases without amyloidosis. Neurosignals. 2008;16(1):41–51.
[16] Thorpe JR, Tang H, Atherton J, et al. Fine structural analysis of the neuronal inclusions of frontotemporal lobar degeneration with TDP-43 proteinopathy. J Neural Transm (Vienna). 2008; 115(12):1661–1671.
[17] Amador-Ortiz C, Lin WL, Ahmed Z, et al. TDP-43 immunoreactivity in hippocampal sclerosis and Alzheimer's disease. Ann Neurol. 2007;61(5):435–445.
[18] Cairns NJ, Neumann M, Bigio EH, et al. TDP-43 in familial and sporadic frontotemporal lobar degeneration with ubiquitin inclusions. Am J Pathol. 2007;171(1):227–240.
[19] Bigio EH, Wu JY, Deng HX, et al. Inclusions in frontotemporal lobar degeneration with TDP-43 proteinopathy (FTLD-TDP) and amyotrophic lateral sclerosis (ALS), but not FTLD with FUS proteinopathy (FTLD-FUS), have properties of amyloid. Acta Neuropathol. 2013;125(3):463–465.
[20] Robinson JL, Geser F, Stieber A, et al. TDP-43 skeins show properties of amyloid in a subset of ALS cases. Acta Neuropathol. 2013;125(1):121–131.
[21] Wang A, Conicella AE, Schmidt HB, et al. A single N-terminal phosphomimic disrupts TDP-43 polymerization, phase separation, and RNA splicing. Embo J. 2018;37(5):e97452.
[22] McGurk L, Gomes E, Guo L, et al. Poly(ADP-Ribose) prevents pathological phase separation of TDP-43 by promoting liquid demixing and stress granule localization. Mol Cell. 2018;71(5): 703–717.e9.
[23] Molliex A, Temirov J, Lee J, et al. Phase separation by low complexity domains promotes stress granule assembly and drives pathological fibrillization. Cell. 2015;163(1):123–133.
[24] Johnson BS, Snead D, Lee JJ, et al. TDP-43 is intrinsically aggregation-prone, and amyotrophic lateral sclerosis-linked mutations accelerate aggregation and increase toxicity. J Biol Chem. 2009;284(30):20329–20339.
[25] Babinchak WM, Haider R, Dumm BK, et al. The role of liquid-liquid phase separation in aggregation of the TDP-43 low-complexity domain. J Biol Chem. 2019;294(16):6306–6317.
[26] Lim L, Wei Y, Lu Y, et al. ALS-causing mutations significantly perturb the self-assembly and interaction with nucleic acid of the intrinsically disordered prion-like domain of TDP-43. PLoS Biol. 2016;14(1):e1002338
[27] Jiang LL, Che MX, Zhao J, et al. Structural transformation of the amyloidogenic core region of TDP-43 protein initiates its aggregation and cytoplasmic inclusion. J Biol Chem. 2013; 288(27):19614–19624.
[28] Guo W, Chen Y, Zhou X, et al. An ALS-associated mutation affecting TDP-43 enhances protein aggregation, fibril formation and neurotoxicity. Nat Struct Mol Biol. 2011;18(7):822–830.
[29] Saini A, Chauhan VS. Delineation of the core aggregation sequences of TDP-43 C-terminal fragment. Chembiochem. 2011;12(16):2495–2501.
[30] Chen AK, Lin RY, Hsieh EZ, et al. Induction of amyloid fibrils by the C-terminal fragments of TDP-43 in amyotrophic lateral sclerosis. J Am Chem Soc. 2010;132(4):1186–1187.
[31] Campioni S, Mannini B, Zampagni M, et al. A causative link between the structure of aberrant protein oligomers and their toxicity. Nat Chem Biol. 2010;6(2):140–147.
[32] D'Andrea C, Foti A, Cottat M, et al. Nanoscale discrimination between toxic and nontoxic protein misfolded oligomers with tip-enhanced Raman spectroscopy. Small. 2018;14(36):e1800890
[33] Chiti F, Bucciantini M, Capanni C, et al. Solution conditions can promote formation of either amyloid protofilaments or mature fibrils from the HypF N-terminal domain. Protein Sci. 2001;10(12):2541–2547.
[34] Bhavsar RD, Shivcharan P, Roy I. Effect of osmolytes on the fibrillation of HypF-N. Biochimie. 2013;95(11):2190–2193.
[35] LeVine H. 3rd. Thioflavine T interaction with synthetic Alzheimer's disease beta-amyloid peptides: detection of amyloid aggregation in solution. Protein Sci. 1993;2(3):404–410.
[36] Klunk WE, Jacob RF, Mason RP. Quantifying amyloid beta-peptide (Abeta) aggregation using the Congo red-Abeta (CR-abeta) spectrophotometric assay. Anal Biochem. 1999;266(1): 66–76.
[37] Calero M, Gasset M. Featuring amyloids with Fourier transform infrared and circular dichroism spectroscopies. Methods Mol Biol. 2012;849:53–68.
[38] Sunde M, Blake C. The structure of amyloid fibrils by electron microscopy and X-ray diffraction. Adv Protein Chem. 1997;50: 123–159.
[39] Gasset-Rosa F, Lu S, Yu H, et al. Cytoplasmic TDP-43 de-mixing independent of stress granules drives inhibition of nuclear import, loss of nuclear TDP-43, and cell death. Neuron. 2019; 102(2):339–357.e7.
[40] Li HR, Chen TC, Hsiao CL, et al. The physical forces mediating self-association and phase-separation in the C-terminal domain of TDP-43. Biochim Biophys Acta Proteins Proteom. 2018; 1866(2):214–223.
[41] Conicella AE, Zerze GH, Mittal J, et al. ALS mutations disrupt phase separation mediated by α-helical structure in the TDP-43 low-complexity C-terminal domain. Structure. 2016;24(9): 1537–1549.
[42] Wang L, Kang J, Lim L, et al. TDP-43 NTD can be induced while CTD is significantly enhanced by ssDNA to undergo liquid-liquid phase separation. Biochem Biophys Res Commun. 2018;499(2):189–195.
[43] Gomes E, Shorter J. The molecular language of membraneless organelles. J Biol Chem. 2019;294(18):7115–7127.
[44] Furukawa Y, Kaneko K, Watanabe S, et al. A seeding reaction recapitulates intracellular formation of Sarkosyl-insoluble transactivation response element (TAR) DNA-binding protein-43 inclusions. J Biol Chem. 2011;286(21):18664–18672.
[45] Cao Q, Boyer DR, Sawaya MR, et al. Cryo-EM structures of four polymorphic TDP-43 amyloid cores. Nat Struct Mol Biol. 2019;26(7):619–627.
[46] Guenther EL, Ge P, Trinh H, et al. Atomic-level evidence for packing and positional amyloid polymorphism by segment from TDP-43 RRM2. Nat Struct Mol Biol. 2018;25(4):311–319.
[47] Eisenberg DS, Sawaya MR. Structural studies of amyloid proteins at the molecular level. Annu Rev Biochem. 2017;86:69–95.
[48] Picotti P, De Franceschi G, Frare E, et al. Amyloid fibril formation and disaggregation of fragment 1-29 of apomyoglobin: insights into the effect of pH on protein fibrillogenesis. J Mol Biol. 2007;367(5):1237–1245.
[49] Ramshini H, Parrini C, Relini A, et al. Large proteins have a great tendency to aggregate but a low propensity to form amyloid fibrils. PLoS One. 2011;6(1):e16075.
[50] Monsellier E, Ramazzotti M, Taddei N, et al. Aggregation propensity of the human proteome. PLoS Comput Biol. 2008;4(10): e1000199.